Polymer 91 (2016) 162–173

Contents lists available at ScienceDirect

Polymer

journal homepage: www.elsevier.com/locate/polymer

Control of molecular curvature and crystallinity of quinacridone-benzoxadiazole copolymers using different π bridge for polymer solar cells

Min-Hee Choi, Hyo Yeol Kim, Eui Jin Lee, Doo Kyung Moon*

Department of Materials Chemistry and Engineering, Konkuk University, 1 Hwayang-dong, Gwangjin-gu, Seoul, 143-701, South Korea

ARTICLE INFO

Article history:
Received 31 December 2015
Received in revised form
14 March 2016
Accepted 20 March 2016
Available online 21 March 2016

Keywords:
Organic solar cells
Molecular engineering
Crystallinity

ABSTRACT

Three quinacridone-benzoxadiazole polymers containing different spacers (PQcOx-T, PQcOx-TT and PQcOx-biT) are obtained via Suzuki coupling reaction to control the energy levels and curvature of the polymer backbones. We find a structural relationship between the polymer backbone and crystallinity, especially regarding packing orientation. PQcOx-T exhibits a zigzag conformation with a dihedral angle over 25° and shows an edge-on structure in pristine film. However, PQcOx-TT exhibits a linear conformation with a dihedral angle under 7° and shows crystallized domains and oriented morphology with shoulder peaks in the UV–vis spectra of both solution and film states. Although PQcOx-biT demonstrates a linear conformation, its electron distribution of both the ground and excited-states are localized on the acceptor unit. Consequently, the intramolecular charge transfer (ICT) effect within PQcOx-biT is poor. Linear polymers prefer regular and crystalline domains in the film state and lead to more efficient organic photovoltaic (OPV) devices. PQcOx-TT possesses a PCE value of up to 3.4%. Further, when we fabricated an inverted device, the PCE increased to 3.6% because of its small surface potential between the active layer and MoO_3. The polymer packing direction and crystallinity were determined by the curvature of the polymer, which suggests an enhancement in charge transport and increases Jsc. Moreover, the small difference of surface potential can possibly improve Voc, FF and PCE.

1. Introduction

Polymer solar cells (PSCs) have received attention from academia and industry as an alternative to inorganic photovoltaic devices. PSCs offer many advantages over such devices, including solution-processability that can reduce manufacturing costs, lightness, flexibility, and suitability to large-scaling [1]. In general, the active layer of PSCs is comprised of a bulk heterojunction (BHJ) configuration, which is a blend of an electron-donor (conducting conjugated polymer) and an electron-acceptor (fullerene derivative) to achieve high efficiency [2,3]. To achieve high-efficiency in a BHJ solar cell, a large number of chemical and structural parameters (e.g., conjugated backbone and side chains) must be judiciously coordinated and managed [4]. In this regard, the donor-acceptor (D-A) concept has been widely used to design the conjugated polymer main chain of PSCs [5–7]. Conjugated polymers, as ideal materials for PSCs, must possess a broad absorption and a high absorption coefficient. In addition, they must have high hole mobility and suitable levels of the highest occupied molecular orbital (HOMO) and lowest unoccupied molecular orbital (LUMO) [8,9]. Along with superior miscibility with fullerene, the polymer and fullerene blend films must also demonstrate effective film forming with nano-structures [10,11]. The power conversion efficiency (PCE) of PSCs has recently reached more than 9–11% by understanding the relationship between the chemical structures of the polymers and their photovoltaic performance [12–16].

The fundamental design of push–pull architectures involves introducing spacers as conjugated π–bridging groups between the donor and acceptor units. New donor and acceptor building blocks have been widely studied, but the π–bridge has only recently received attention. The conjugated π–bridge greatly influences the electronic structure of push–pull polymers by contributing to the density and electronic interaction (i.e., molecular orbitals) of the π-

* Corresponding author. Present address: Department of Materials Chemistry and Engineering, Konkuk University, 1 Hwayang-dong, Gwangjin-gu, Seoul, 143-701, South Korea.
E-mail address: dkmoon@konkuk.ac.kr (D. Kyung Moon).

http://dx.doi.org/10.1016/j.polymer.2016.03.062
0032-3861/

electrons. The typical spacers used include vinylenes [17], thiophenes [18,19], furans, and selenophenes [20]. However, in recent years, more attention has been given to multiple thiophenes (such as bithiophene or terthiophene) [21] and thieno [3,2-b]thiophene [22], which is a fused aromatic ring. As the number of thienyl (T) spacers increases, the polymer backbone can achieve superior planarity and improved conjugation length. This leads to a red-shifted absorption area, reduces the band gap, and increases the charge mobility. Previously, our research group synthesized D–π–A type polymers of poly [alkylidenefluorene-alt-di(thiophene)n-isoindigo] (n = 0–2) and reported that a change in the steric hindrance of the polymers and its orientation depend on the number of thiophene spacers [23]. In most semiconducting organic materials that exhibit electric charges move effectively along the π-stacking direction, which is an anisotropic charge transport [24,25]. Particularly in PSC, the face-on structure is more advantageous for the transfer of electric charge than the edge-on structure. Thieno [3,2-b]thiophene has a centrosymmetric, rigid, and coplanar structure. Thus, this structure delocalizes π-electrons along the polymer backbone with enhanced intermolecular π–π stacking [26]. Mats R. Andersson, Wei W. and Jianhui Hou groups have published the results of efforts to improve the planarity of polymers by introducing thieno [3,2-b]thiophene as a spacer between a benzodithiophene donor unit and a quinoxaline acceptor unit [27,28].

To achieve close packing of the polymers and thus good charge transport characteristics, the energetic disorder must be reduced by increasing the coplanarity and intermolecular 2D π–π interactions. One of the appropriate candidates for achieving this objective is the quinacridone (QC) derivative. The QC derivative (well-known as a red-violet pigment), with a lattice and self-assembly characteristics, has been widely applied in organic thin film transistors (OTFTs) because of its excellent mobility. The Takimiya group has recently reported a high hole mobility (0.2 $cm^2 V^{-1} S^{-1}$) in OTFTs based on QC derivatives [29].

Benzothiadiazole (BT) and benzoxadiazole (BO) are among the well-known strong acceptors in D-A type polymers. In particular, BT-based polymers are one of the most important conducting polymers because of their easy synthetic process, good stability, and electro-optical characteristics [10,30]. However, relatively little research has been conducted on PSCs and OTFTs utilizing BO-based conjugated polymers. This is because early researchers who studied BO-based polymers were disappointed with their low molecular weights and poor solubility compared to BT-based polymers [31]. However, because oxygen atom has a higher electronegativity than sulfur, BO unit-based polymers have a deeper HOMO level than BT-based polymers. As a result, BO unit-based polymers are expected to be highly air-stable, and a high open circuit voltage (Voc) can be expected [32–34].

Here, D-π-A-type polymers were synthesized based on a QC derivative with a unique π–bridge structure. Additionally, the curvature and the optical, electrochemical properties of the polymers based on the spacer structures were characterized. The results showed that the introduction of a long spacer reduced the twist angle between the acceptor and donor, thus enhancing the planarity and crystallinity of the polymers. However, it was confirmed that excessive elongation of the π–bridge in DA-type polymers with a weak donor undermines the electron donating property of the donor and eventually reduces the ICT. When an active layer was introduced by the polymer containing thieno [3,2-b]thiophene as the spacer, the conventional cell had the highest short circuit current (Jsc), with a power conversion efficiency (PCE) of 3.4%. In the case of the inverted cell, the polymer containing thiophene (with the highest Voc) as the spacer exhibited the highest efficiency of 3.6%.

2. Results and discussion

2.1. Synthesis and characterization of polymers

The chemical structures of the monomers and polymers and their synthetic procedures are shown in Scheme 1. The monomers used in this study contain 2,9-diboronicester-N,N′-di(2-octyldodecyl)quinacridone (D1) [35] as a donor and 5,6-bis(octyloxy) benzo[c] [1,2,5]oxadiazole (A0) [36] as a well-known strong acceptor, each of which was synthesized according to previously reported methods. In addition, according to previously reported procedures, thiophene, 2,2'-bithiophene and thieno [3,2-b]thiophene were adopted as spacers for A0 to synthesize, respectively, 4,7-bis(5-bromothiophen-2-yl)-5,6-bis(octyloxy)benzo[c] [1,2,5] oxadiazole (A1) [37], 4,7-bis(5-bromothieno [3,2-b]thiophen-2-yl)-5,6-bis(octyloxy)benzo[c] [1,2,5]oxadiazole (A2) [22], and 4,7-bis(5'-bromo-2,2'-bithiophen-5-yl)-5,6-bis(octyloxy)benzo[c] [1,2,5]oxadiazole (A3) [38], as shown in Scheme 1. Poly [quinacridone-alt-spacer-bis (octyloxy)benzo[c] [1,2,5]oxadiazole] (PQcOx-T, PQcOx-TT, and PQcOx-biT) were synthesized via the Suzuki coupling reaction using D1 and benzo[c] [1,2,5]oxadiazole derivatives (A1~A3). Polymerization was performed with toluene as the solvent, $Pd(PPh_3)_4(0)$ as the catalyst, 2 M aqueous potassium carbonate solution as the base, and Aliquat 336 as the surfactant for 48 h at 90–95 °C. After polymerization, end-capping was performed with bromobenzene and phenylboronic acid for 3 h each. The obtained powders were collected by re-precipitation into methanol, and were purified using a Soxhlet apparatus using methanol, acetone, and chloroform in sequence. Finally, the chloroform-soluble portion was recovered by re-precipitated in methanol. All powders obtained were black-purple solids with yields of 90%, 78%, and 95% for PQcOx-T, PQcOx-TT, and PQcOx-biT, respectively. PQcOx-T and PQcOx-biT dissolved easily in common organic solvents such as chloroform ($CHCl_3$), tetrahydrofuran (THF), chlorobenzene, and o-dichlorobenzene. However, PQcOx-TT dissolved completely only at elevated temperatures.

The structures of the synthesized polymers were identified using ^1H NMR spectra and elemental analysis (EA) (See ESI, Fig. S1). PQcOx-T exhibited peaks attributed to hydrogen atoms bonded to the carbon atoms of the introduced aromatic quinacridone and thiophene spacers in the ranges of 8.85–8.03 ppm and 7.68–7.20 ppm, respectively. In the case of PQcOx-biT, where only the spacer was modified from thiophene to bithiophene, peaks of hydrogen atoms bonded to aromatic carbon atoms were observed in the ranges of 8.61–8.16 ppm, 7.62–7.52 ppm, and 7.21–6.76 ppm; the location of the peaks is similar to that of PQcOx-T. The number of aromatic hydrogen atoms observed increased by 4 for PQcOx-biT compared to PQcOx-T. The NMR spectra of PQcOx-TT exhibited broadened peaks with lower resolution than those of PQcOx-T and PQcOx-biT because PQcOx-TT has limited solubility in $CDCl_3$ at room temperature. Elemental analysis of PQcOx-TT gave values of C = 73.54, H = 8.44, N = 3.52, O = 5.14, and S = 8.43, which are more than 96% consistent with the theoretical values of C = 74.18, H = 8.82, N = 3.60, O = 5.15, and S = 8.25.

The measured polymer molecular weights are listed in Table 1. As shown, the number average molecular weights (Mn) of PQcOx-T, PQcOx-TT, and PQcOx-biT were 34.8, 43.1, and 43.3 kDa, respectively, with broad PDIs of 1.75, 2.31, and 2.10. Mats R. Andersson et al. reported that the degree of polymerization declines because the thieno [3,2-b]thiophene spacer-based acceptor is generally less soluble than the thiophene spacer-based acceptor [27]. However, in this study, PQcOx-TT was observed to have a similar degree of polymerization to that of PQcOx-T and PQcOx-biT. This is because no differences in the solubility of A1~A3 were observed on account of the introduction of the octyloxy side chain into 5, 6-C of benzo[c]

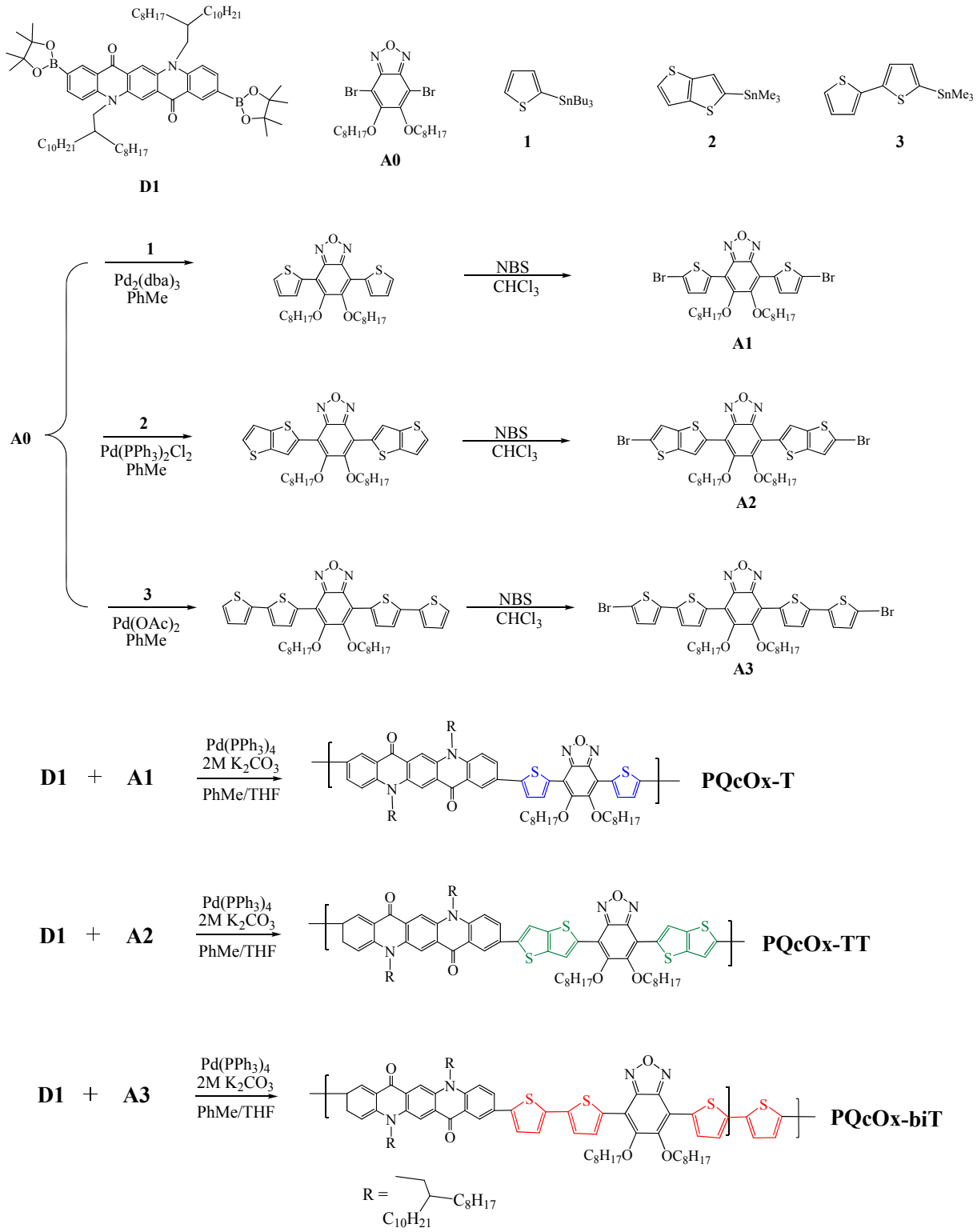

Scheme 1. Synthetic route to the polymers.

[1,2,5]oxadiazole, which is an acceptor.

Fig. S2 shows the TGA measurements of all polymers, the temperatures of which at 5% thermal weight loss in N_2 atmosphere were 300 °C or higher. The obtained polymers exhibited good thermal stability, and proved to be suitable for device fabrication and application.

2.2. Optical properties

The normalized UV–visible spectra of the polymers in chloroform and an as-cast thin film are presented in Fig. 1 to examine the effects of the spacer structures on the optoelectronic properties of the quinacridone-based polymers. The results are summarized in

Table 1
Physical and thermal properties of the polymers.

Polymer	Yield [%]	Mn[a] [kDa]	Mw[a] [kDa]	PDI[a]	Degree of polymerization	T_d [°C]
PQcOx-T	90	34.8	61.0	1.75	24	310
PQcOx-TT	78	43.1	99.6	2.31	28	303
PQcOx-biT	95	43.3	91.0	2.10	27	300

[a] Determined by GPC in tetrahydrofuran (THF) using polystyrene standards.

Table 2. The molar absorption coefficients (ε, λ_{max}) of the polymers are summarized in Fig. S3 (See ESI).

As shown in Fig. 1, all polymers exhibit two absorption peaks in the range of 300–800 nm. The peak in the high energy band (400–500 nm) is caused by the π– π* transition of the donor segments (quinacridone group), whereas the peak in the low energy band (500–700 nm) is caused by the intramolecular charge transfer (ICT) transition between the donor and acceptor [39].

The maximum absorption peak (λ_{max}) with the highest intensity of solution-phase PQcOx-T was observed at 528 nm, with a calculated absorption coefficient of $8.5 \times 10^4\ M^{-1}\ cm^{-1}$. In the case of the film phase, the maximum absorption peak was red-shifted by 5 nm ($\lambda_{max} = 533$ nm) compared to the solution phase. This implies that effective 2D-stacking was achieved because the intermolecular interaction is stronger in the film phase than in the solution phase. The absorption edge of PQcOx-T was 599 nm, and the optical band gap was calculated to be 2.07 eV from this edge. This is the largest value for the polymers synthesized in this study. Therefore, this observation suggests that the largest bandgap can be obtained when the thiophene spacer is introduced into the main chain, resulting in the correspondingly narrowest absorption band. The λ_{max} of PQcOx-TT in the solution phase was observed at 550 nm, with a calculated absorption coefficient of $13.7 \times 10^4\ M^{-1}\ cm^{-1}$. This value is greater than those for the PQcOx-T and PQcOx-biT polymers, indicating that PQcOx-TT facilitates greater optical absorption. The $\lambda_{max}$was observed to be blue-shifted by 3 nm ($\lambda_{max} = 547$ nm) in the film phase relative to the solution phase. The absorption edge of PQcOx-TT was at 663 nm, from which the optical bandgap was calculated to be 1.87 eV. In addition, the absorption spectra of PQcOx-TT were red shifted by 22 nm in the solution phase and by 14 nm in the film phase relative to those of PQcOx-T. This confirmed that the absorption bands became broader as the length of the spacer introduced between the quinacridone donor unit and the benzo[c] [1,2,5]oxadiazole acceptor unit increased; that is, PQcOx-TT had broader absorption bands than PQcOx-T, and the bandgap was reduced. The reduction of the bandgap can be explained by the increased effective conjugation length of the polymers [40]. The λ_{max} of PQcOx-biT in the solution phase was found at 556 nm, with a calculated absorption coefficient of $5.1 \times 10^4\ M^{-1}\ cm^{-1}$. The maximum absorption peak ($\lambda_{max} = 558$ nm) of PQcOx-biT was red-shifted by 2 nm in the film phase relative to the solution phase. The absorption edge of PQcOx-biT was at 700 nm, and the optical bandgap was calculated to be 1.77 eV. This is the smallest bandgap for the polymers synthesized in this study. These results are similar to the findings of other researchers such as David G. Lidzey and Erjun Zhou [41,42].

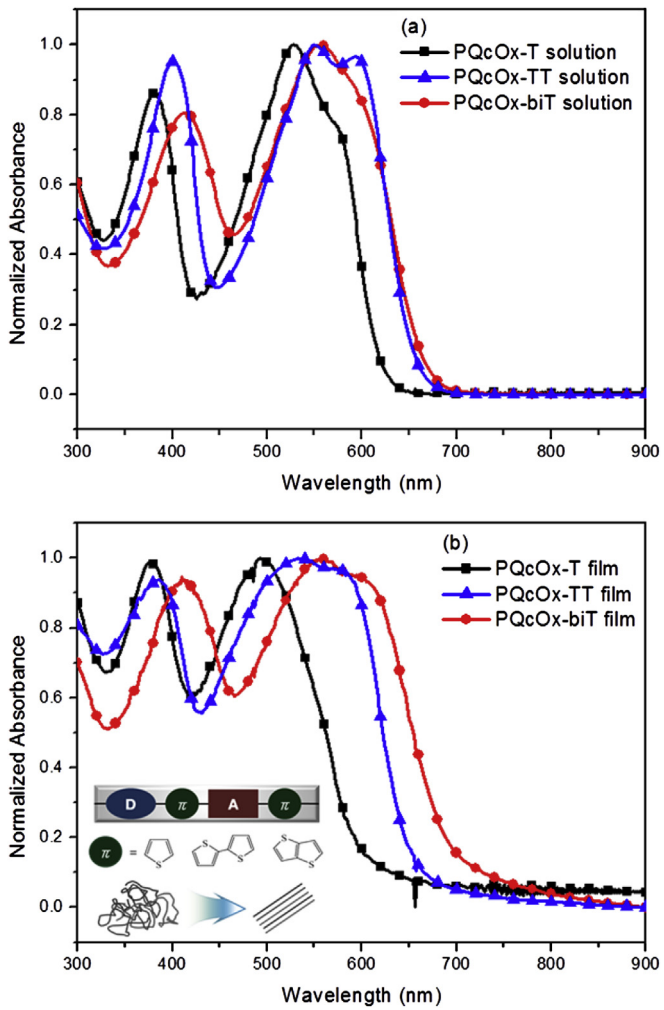

Fig. 1. UV–vis absorption spectra of the polymers in solution (a) and film (b).

These three polymers exhibited different absorption characteristics for the ICT transition-induced absorption peak (600–750 nm) depending on the spacer structures. PQcOx-T showed a weak absorption shoulder peak(λ_{sh}) at 572 nm in the solution phase, whereas the λ_{sh} disappeared in the film phase. The shoulder absorption occurs because of stacking of the polymer chains [41,43]. It indicated that PQcOx-T has the π–π stacking interactions between polymer chains in solution state. However, the shoulder absorption doesn't exist in PQcOx-T film. It meant that the chain linearity and planarity of PQcOx-T break up, and the crystalline intermolecular organization disrupts in film state [44]. Therefore, it is deduced that the π–π stacking interactions between the polymer chains of PQcOx-T in film state are weakened because the distances between the polymers decreased. In contrast, PQcOx-biT did not show a shoulder peak in the solution phase, whereas it showed an absorption shoulder peak at 598 nm in the film. This is because the bithiophene spacer creates a more planar conformation in the main chains of the polymer between the donor unit and the acceptor unit relative to the thiophene spacer, and thus the bithiophene spacer induces orderly π–π stacking. Because the intermolecular distance decreases more in the film phase than in the solution phase, polymers with high planarity have stronger intermolecular interactions because of their aggregation in the solid state. PQcOx-TT showed a strong shoulder peak in both the solution ($\lambda_{sh} = 593$) and thin film phases ($\lambda_{sh} = 592$ nm), which confirmed that the orderly π–π stacking or strong aggregation between the polymer chains

Table 2
Optical and electrochemical data of the polymers.

Polymer	UV–vis absorption					E_g^{op}, [a] [eV]	Cyclic voltammetry		
	$CHCl_3$ solution [nm]		Film [nm]				E^{ox}_{onset} [V]	HOMO[b] [eV]	LUMO[c] [eV]
	λ_{max} [nm]	λ_{sh} [nm]	λ_{max} [nm]	λ_{sh} [nm]	λ_{onset} [nm]				
PQcOx-T	379, 528	572	382, 533	–	599	2.07	1.07	−5.34	−3.27
PQcOx-TT	401, 550	593	396, 547	592	663	1.87	1.03	−5.30	−3.43
PQcOx-biT	414, 556	–	410, 558	598	700	1.77	1.00	−5.26	−3.49

[a] Calculated from the intersection of the tangent on the low energetic edge of the absorption spectrum with the baseline.
[b] $E_{HOMO} = -[E_{onset(vs\ Ag/AgCl)} - E_{1/2(Fc/Fc+\ vs\ Ag/AgCl)}] - 4.8$ eV.
[c] $E_{LOMO} = E_g - E_{HOMO}$.

could also be achieved in dilute solutions [45,46]. Previous studies have indicated that the conjugation of the polymer main chain increases effectively by enhancing the coplanarity between the donor and acceptor via the introduction of thieno [3,2-b]thiophene spacers. Researchers such as Xiaoyu Li, Yongfang Li, and Haiqiao Wang reported that the introduction of thieno [3,2-b]thiophene as a π-bridge changed the z-shaped molecular chains into almost a linear configurations compared with furan or thiophene [32]. Furthermore, our research group synthesized a quinacridone-based D–π–A type polymer and reported that the coplanar property of the polymers varied depending on the type of acceptor and the location of the side chain. Based on these results, the quinacridone-based D–π–A type polymer in which benzothiadiazole and phenazine derivatives were introduced as acceptors showed absorption shoulder peaks in the UV–vis absorption spectra both in the solution and film phases. The XRD patterns showed that the film creates a face-on structure in these polymers [47,48]. In contrast, the quinacridone-based polymer consisting of quinoxaline or thiophene derivatives did not exhibit an λ_{sh} in the UV–vis absorption spectra, or such a peak was observed only for the film phase, which caused the polymer thin film to form an amorphous or edge-on structure [35,49].

The absorption coefficient of PQcOx-TT is approximately 1.6–2.7 times larger than that of the other two polymers. This means that PQcOx-TT is capable of exhibiting enhanced optical absorption. The high molar absorption coefficient of PQcOx-TT is attributed to the excellent planarity of the polymer. Because planar, high molecular weight polymers have strong intermolecular π–π stacking interactions, this arrangement is advantageous for its charge transfer character and π–π* electron transitions. As a result, the polymers show exceptionally high molar absorptivity. This is consistent with the findings of Huriye Icil et al. and Wenjun Yang et al. [50,51].

2.3. Computational study

To gain a deeper understanding of the molecular geometries and electron density of states distribution, as well as the electronic properties of the synthesized polymers, simulations were performed using density functional theory (DFT). DFT calculations were performed using Gaussian 09 with the hybrid B3LYP correlation functional and the split valence 6-31G(d) basis set. For the purpose of computational simplification, the alkoxy side chains on the benzo[c] [1,2,5]oxadiazole acceptor unit were replaced with butoxy groups, and the branched alkyl side chains on the quinacridone unit were replaced with sec-butyl groups. The polymer backbones were simplified into oligomers with two repeating units prior to the calculations. The obtained HOMO and LUMO orbitals are presented in Fig. S4 and Table 3.

The LUMO orbitals shown in Fig. S4 are localized on the acceptor unit containing benzo[c] [1,2,5]oxadiazole and the spacer.

This is because of the quinoid structural characteristics created between the sulfur and nitrogen atoms that have non-bonding electron pairs and electron-withdrawing properties. The HOMO orbitals are distributed over the polymer main chain depending on the type of spacer. The HOMO of PQcOx-T was localized on quinacridone, whereas the HOMO of PQcOx-TT was delocalized over the entire polymer chain. In the case of PQcOx-biT, the electron cloud of the HOMO orbital was localized on the acceptor unit. This is because as the spacer is converted into thiophene, thieno [3,2-b] thiophene, and 2,2'-bithiophene (T → TT → biT), it has stronger electron-donating properties than quinacridone, which is a weak donor. The results of the DFT calculations show that PQcOx-T and PQcOx-TT have a well-defined D–π–A structure and intramolecular charge transfer properties (i.e., the HOMO to LUMO transition is a donor to acceptor intramolecular charge transfer). In the case of PQcOx-biT, however, the ICT effect is unlikely to proceed smoothly because both the ground-state and excited-state electrons exist in the same location.

In the optimized geometries of the backbones of the three polymers determined through DFT shown in Fig. S4, PQcOx-T shows a typical zigzag conformation (angle = 136.4°, Z-type). PQcOx-T has a planar interior of repeating units (angle = 172.8°), but has a large torsional angle in the linker region connecting the repeating units. In contrast, PQcOx-TT and PQcOx-biT adopted an almost straight conformation (L-type). PQcOx-TT has 147.6° and 153.7° torsional angles between quinacridone and benzoxdiazole at interior and linker region of repeating unit, respectively. PQcOx-biT has 134.2° and 147.5° torsional angles. These polymers have unvarying torsional angles both interior and linker region of repeating units. This indicates that the polymer backbone conformations can be adjusted by introducing thieno [3,2-b]thiophene (TT) and 2,2'-bithiophene (biT) as the π-bridge units instead of thiophene (T) [28]. This is in agreement with the observed disappearance of the shoulder peaks in the UV–vis absorption spectrum of PQcOx-T because of the decreased π–π interaction in the film phase, whereas shoulder peaks of PQcOx-TT and PQcOx-biT appear in the film phase. Moreover, dihedral angles 1 and 3 between the quinacridone unit and spacer groups, summarized in Table 3, which range from 22.35° to 27.41°, demonstrated similar values for the three polymers. In contrast, dihedral angle 2 between the spacer and oxadiazole unit was smaller for PQcOx-TT, being as low as 30% (θ2 = 6.52°) of the other polymers. This results from the changes in the torsional angle between the moieties (thiophene or

Table 3
Calculated parameters.

Polymer	Dihedral angle (deg)			HOMO[cal.] [eV]	LUMO[cal.] [eV]
	1	2	3		
PQcOx-T	26.03	21.42	25.15	−5.22	−2.72
PQcOx-TT	27.41	6.52	26.03	−5.19	−2.77
PQcOx-biT	22.35	18.98	24.70	−5.02	−2.77

thienothiophene) contiguous to the alkoxy Ox. In other words, the minimum energy geometry of the polymers is more planar and linear because of the attractive Coulombic interactions between C–H···N and S···O when the thienothiophene spacer is introduced [52]. Stronger steric hindrance (twisting of the conjugated backbone) essentially breaks the conjugation at the linkages, which contribute negligible π–π stacking of the intermolecular interaction and decreases charge transport [53]. Increased dihedral angle reduces the current by breaking conjugation in the fabrication of devices. Therefore, the current of PQcOx-TT, which possesses the smallest dihedral angle, is expected to be the highest in the fabricated organic photovoltaic (OPV) cell.

The highest occupied molecular orbital (HOMO) levels of PQcOx-T, PQcOx-TT, and PQcOx-biT were calculated to be −5.22, −5.19, and −5.02 eV, respectively. The HOMO levels determined from the DFT calculation tended to increase as the conjugation length and electron donating property of the donor segments increased. This is consistent with the findings by You et al., who reported that the HOMO energy level is determined by the donor strength in a push–pull system [5]. This is because the donor strength increases as the number of spacers increase and as the spacer becomes more coplanar. This result is also consistent with that reported by Lidzey and Jianhui Hou et al., whereby the HOMO level increased because of the electron-donating properties of the thiophene spacer [38,54,55].

2.4. X-ray diffraction (XRD) measurements

To gain a better understanding of the ordering and crystallinity of the polymer thin films according to the spacer structure, X-ray diffraction measurements was performed with their associated annealing temperatures.

The X-ray diffraction pattern of the polymer films acquired in the out-of-plane mode is presented in Fig. 2(a) to scrutinize the ordering structure of the polymer. The (h00) diffraction peaks of the PQcOx-T and PQcOx-biT thin films acquired in the out-of-plane mode appeared at 3.87° and 4.58°, respectively. Based on the calculation using Bragg's law (i.e., $\lambda = 2d\sin\theta$), the highly ordered (100) lamellar d-spacings (d_1) were 22.85 and 19.29 Å for the respective polymers, which implies that the two polymers form a (h00) lamellar structure. The (0h0) peak was not observed. In contrast with the PQcOx-T and PQcOx-biT polymers, PQcOx-TT had diffraction peaks at 4.26° and 25.05°. This suggests that the polymer adopts a (h00) lamellar structure combined with a (0h0) lamellar structure. According to the calculation using Bragg's law, the highly ordered (100) lamellar d-spacing (d_1) was 20.74 Å and the π–π stacking distance (d_π) was 3.55 Å. Therefore, if the π–π stacking peak is observed for the (010) plane in the out-of-plane mode, the crystal structure of the PQcOx-TT polymer thin film is likely to adopt a face-on orientation. This can be confirmed through X-ray diffraction measurements of the in-plane mode. An X-ray diffraction analysis of the PQcOx-T, PQcOx-TT, and PQcOx-biT polymer thin films measured in the in-plane mode is presented in Fig. 2(b). The measurements acquired in the in-plane mode showed no diffraction peaks for the PQcOx-T and PQcOx-biT thin films for which no (0h0) peak was observed in the out-of-plane mode. In contrast, the spectrum of PQcOx-TT showed crystal peaks in both the high and low angles and in the in-plane mode.

The aforementioned XRD data imply that PQcOx-T and PQcOx-biT have edge-on structures in the thin film, whereas PQcOx-TT has a bimodal-type crystal structure in which edge-on and face-on crystallites coexist in the polymer film, as in Fig. 2(c) [56]. This is consistent with the disappearance of the shoulder peak in the UV–vis absorption spectra because of the decreased intermolecular interaction of PQcOx-T in the film configuration and the observation of a shoulder peak for PQcOx-TT in both the solution and film

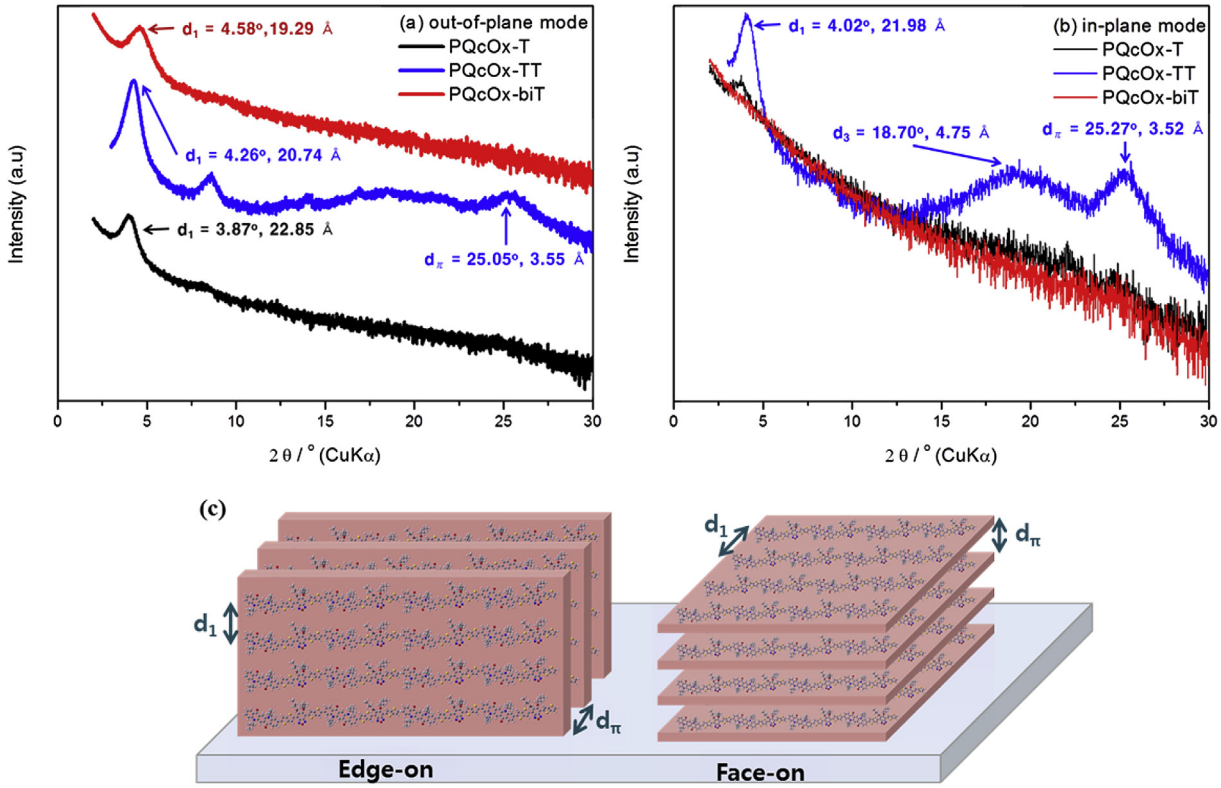

Fig. 2. X-ray diffraction pattern of the polymers on silicon wafers out-of-plane (a), in-plane (b) and schematic morphology of PQcOx-TT (c).

phases [57]. Moreover, it was confirmed that the extended length of the spacers from PQcOx-T to PQcOx-biT decreases the d_1-spacing (which is the intermolecular distance between polymers) from 22.85 Å to 19.29 Å. This is because the distance between the quinacridone and benzo[c] [1,2,5]oxadiazole cores increases as the spacer length increases, allowing more space for side chains to penetrate [58].

2.5. Electrochemical properties

Cyclic voltammetry (CV) was produced using a Zahner IM6eX electrochemical workstation with the polymer film on a Pt plate as the working electrode, an ITO glass as the counter electrode, and silver/silver chloride [Ag in 0.1 M KCl] as the reference electrode in a 0.1 M tetrabutylammonium hexafluorophosphate (Bu_4NPF_6) acetonitrile solution. The constant scan rate was 50 mV/s.

To identify the effects of the spacer structures on the energy level difference, cyclic voltammograms of the PQcOx-T, PQcOx-TT, and PQcOx-biT polymer thin films were measured using a 0.1 M tetrabutylammoniumhexa fluorophosphate (Bu_4NPF_6) acetonitrile solution. The results are presented in Fig. 3 and summarized in Table 2.

The oxidation onset potentials (E^{ox}_{onset}) of PQcOx-T, PQcOx-TT, and PQcOx-biT were +1.07, +1.03, and +1.00 V, respectively; and the calculated HOMO levels were −5.34, −5.30, and −5.26 eV, respectively. Because the air oxidation threshold is −5.27 eV, the materials must have lower HOMO levels than this threshold to achieve oxidative stability. PQcOx-T and PQcOx-TT with lower HOMO levels (−5.27 eV or lower) are expected to have excellent oxidative stability.

As the conjugation length of the spacer unit increased and the electron donating properties became stronger, the HOMO energy level of the polymers tended to increase, moving from −5.34 eV to −5.26 eV. This result is consistent with the polymer energy levels predicted by DFT calculations.

2.6. Photovoltaic properties

BHJ PSCs were fabricated to investigate the photovoltaic (PV) properties of the synthesized polymers. The structure of PSC devices are shown in Fig. 4(a). The polymer/$PC_{70}BM$ weight ratios used in the measurement were 1:1 and 1:2, allowing for variation, and dichlorobenzene (DCB) was used as a solvent. The four separate devices were tested under all stated conditions. The J-V curves acquired using the optimized weight ratios of the PQcOx-T, PQcOx-TT, and PQcOx-biT polymers are shown in Fig. 4(b), (c) and (d), and their incident photon to current conversion efficiency IPCE profiles are presented in Fig. 4(e), (f) and (g). The PV properties of the fabricated PSCs are summarized in Table 4.

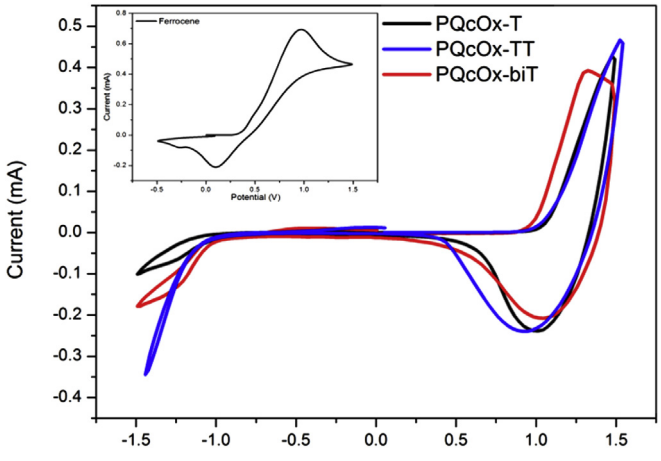

Fig. 3. Cyclic voltammograms of the polymers.

In the case of conventional cell, for PQcOx-T, the open circuit voltage (V_{oc}) was 0.80 V, the short-circuit current density (J_{sc}) was 6.3 $mAcm^2$, and the fill factor (FF) was 47.7%, with a PCE of 2.4%. For PQcOx-TT, the V_{oc} was 0.72 V, the J_{sc} was 7.8 mA/cm^2, and the FF was 43.5%, with a PCE of 2.5%. For PQcOx-biT, the V_{oc} was 0.72 V, the J_{sc} was 4.6 mA/cm^2, and the FF was 46.7%, with PCE = 1.4%.

The V_{OC} is determined by the difference between the HOMO energy level of the polymer and the LUMO energy level of PCBM. The V_{OC} of the fabricated devices followed a similar trend to that of the HOMO levels determined from DFT and CV. As the donor strength increased, the HOMO energy level was upshifted and the V_{OC} values were lowered. PQcOx-TT had the most planar structure and a high adsorption coefficient. Further, PQcOx-TT establishes an ordered crystalline morphology in the film phase, which has a face-on enriched structure. Therefore, PQcOx-TT showed the highest J_{sc}. In contrast, PQcOx-T and PQcOx-biT created an amorphous structure. In particular, PQcOx-biT demonstrated poor intramolecular charge transfer, resulting in a decreased J_{sc} (6.3 and 4.6 mA/cm^2 for PQcOx-T and PQcOx-bi, respectively).

In recent years, poly[(9,9-bis(3'-(*N*,*N*-dimethylamino)propyl)-2,7-fluorene)-alt-2,7-(9,9-dioctylfluorene)] (PFN) has been introduced as an interlayer to improve the device performance in many studies because PFN enhances electron transport and the interfacial adhesion between the active layers and cathodes [49,59]. Therefore, we fabricated the devices by introducing PFN into a device with an optimized ratio. The performance of the devices with PFN improved because of the increased J_{sc} and FF relative to the device without PFN, which we attribute to enhanced electron transport between the active layers and Al in the device with PFN. Compared with the devices without PFN layer, the PCEs of the devices with PFN were increased by 21–100%. PQcOx-TT resulted in the highest level of efficiency when the PFN interlayer was introduced, with a PCE of 3.4%, V_{oc} of 0.76 V, J_{sc} of 8.1 $mAcm^2$, and a FF of 51.9%.

In this study, the inverted devices were fabricated and their characteristics were evaluated to optimize the device structures and to improve the device performance. Compared with conventional devices, inverted type devices demonstrate better long-term ambient stability by phase separation along the vertical direction and concentration dispersion of the active layer. There have been extensive investigations of PSCs with an inverted device structure to enhance both stability and PCE [60]. The J-V curves of the inverted solar cells at the optimized weight ratio of the polymers are presented in Fig. 4(d), and their IPCE profiles are shown in Fig. 4(g). The PCE of inverted devices with PQcOx-T and PQcOx-TT were increased to 3.4% and 3.6%, respectively. The improved performance of the two polymers is attributed to the higher V_{oc} (0.80–0.82 V → 0.86 V, 0.72–0.76 V → 0.78 V) and FF (47.7–50% → 57.6%, 43.5–51.9% → 59.1%).

It is well known that the work functions of hole extraction layers play an important role in the overall performance of inverted organic solar cells because of the energy level alignment of the donor material and metal anode. The surface potential difference (ΔSP) of the polymer:$PC_{70}BM$ vs. PEDOT:PSS and polymer:$PC_{70}BM$ vs. MoO_3 films were measured via EFM to identify the energy level matching between the active layer and HTL layers [61]. In conventional structure, the samples were prepared by drop casting a small amount of polymer:$PC_{70}BM$ blend solution onto the PEDOT:PSS films and then letting it spread slowly while it dried to form the interface [61]. The corresponding surface potential images of polymer:$PC_{70}BM$ – PEDOT:PSS are shown in Fig. S5. At the interface of the two layers, ΔSP of the two distinct parts changed

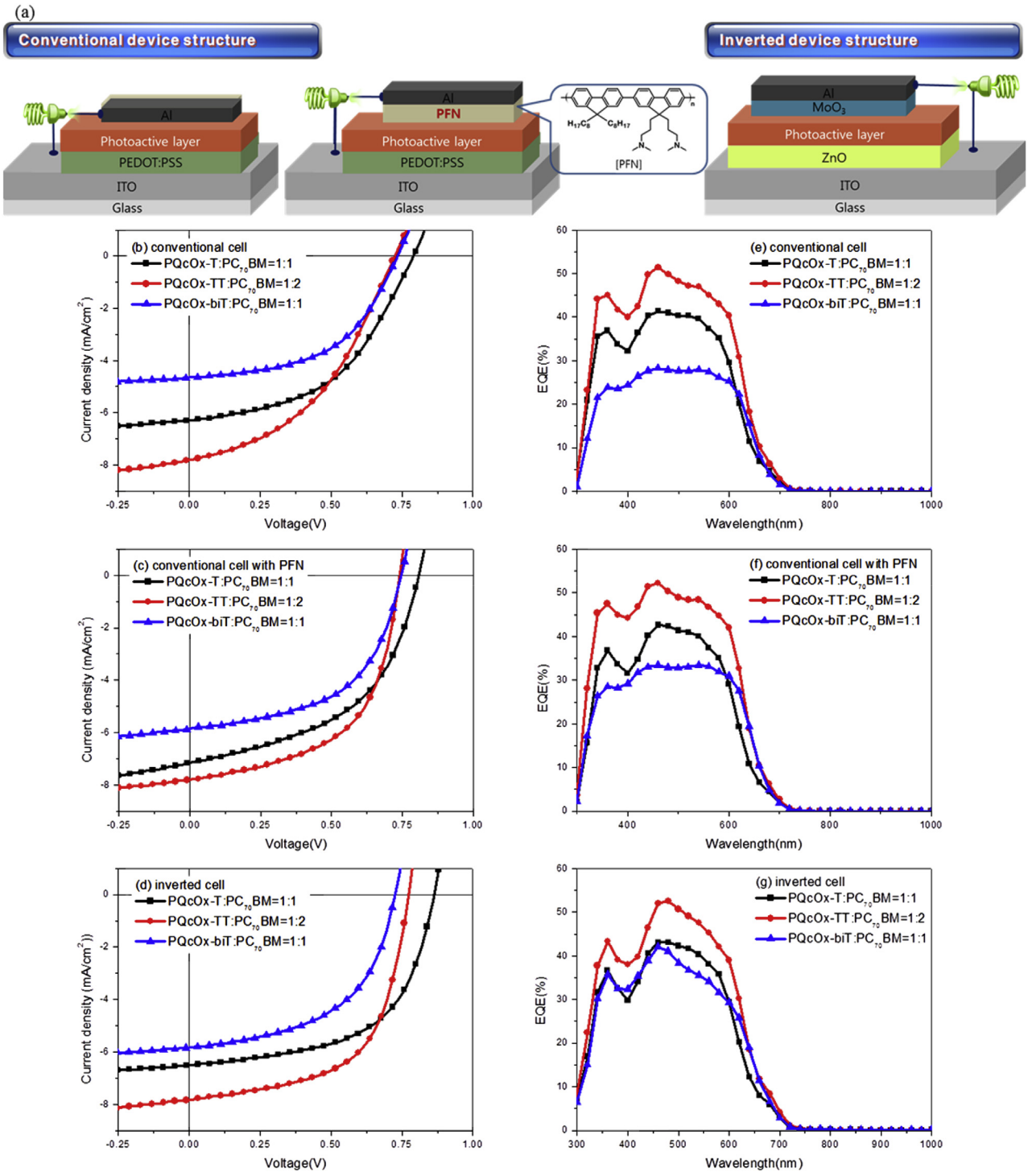

Fig. 4. The conventional and inverted device structure of organic photovoltaic solar cells (a). The J–V curves of the PSC based on Polymer: $PC_{70}BM$ (b), (c), (d) under the illumination of AM 1.5G, 100 mW/cm^2. The IPCE spectra of the PSC based on Polymer: $PC_{70}BM$ (e), (f), (g).

from 6.59 to 9.79 mV depending of the kind of donor polymers. PQcOx-TT had the smallest ΔSP, while PQcOx-biT showed largest ΔSP. In inverted structure, samples were prepared by spin-coating on the ZnO with the polymer:$PC_{70}BM$ blend solution followed by partial thermal evaporation of MoO_3. The corresponding surface potential images of polymer:$PC_{70}BM$ – MoO_3 are shown in Fig. 5. At the interface of the two layers, ΔSP of the two distinct parts displayed a similar tendency towards ΔSP of polymer:$PC_{70}BM$ – PEDOT:PSS. PQcOx-TT showed the smallest ΔSP of 0.80 mV. This implies that the small potential difference between the active layer and HTLs facilitated the hole extraction and also increased the probability of dissociation of excitons into free charge carriers, resulting in the improved V_{oc} and FF [45]. ΔSP of polymer:$PC_{70}BM$ – PEDOT:PSS was larger than polymer:$PC_{70}BM$ – MoO_3. It is well matched by the enhanced V_{oc} and FF in inverted solar cell.

These devices had sufficiently broad external quantum

Table 4
Photovoltaic properties of the polymers.

Polymer	Device structure	$PC_{70}BM$ ratios	V_{oc} [V]	J_{sc} [mA/cm^2]	FF [%]	PCE [%]
PQcOx-T	Conventional	1:1	0.80	6.3	47.7	2.4
	Conventional	1:1 with PFN	0.82	7.2	50.0	2.9
PQcOx-TT	Conventional	1:2	0.72	7.8	43.5	2.5
	Conventional	1:2 with PFN	0.76	8.1	51.9	3.4
PQcOx-biT	Conventional	1:1	0.72	4.6	46.7	1.4
	Conventional	1:1 with PFN	0.74	5.8	54.8	2.4
PQcOx-T	Inverted	1:1	0.86	6.5	57.6	3.4
PQcOx-TT	Inverted	1:2	0.78	7.8	59.1	3.6
PQcOx-biT	Inverted	1:1	0.72	5.9	53.4	2.4

efficiency (EQE) in the visible range. High EQE values were observed in the range of 300–750 nm, which is the absorption region, but the values were lowered at above the 750 nm region. In particular, the PQcOx-TT:$PC_{70}BM$-based device showed the highest EQE (up to 52.8%) at 460 nm, whereas PQcOx-T and PQcOx-biT produced values of 41.4% and 35.5%, respectively. This is consistent with the absorption coefficient and the photocurrent value. When we manufactured inverted PSC devices, all three polymers had similar Jsc values of conventional cells. As shown in the EQE spectra of inverted PSC in Fig. 4(g), no change is observed in the photon-electron conversion along the entire spectrum.

2.7. Hole mobility and morphological properties

In BHJ solar cells, Jsc and FF are directly limited by the hole mobility of the polymer; thus, it is a very important parameter for photovoltaic performance. We determined the hole mobility of the polymer and $PC_{70}BM$ blend films from the $\ln(JL^3/V^2)$ vs. $(V/L)^{1/2}$ graph presented in the ESI* (Figs. S6–S8, Table S1) via a space charge limited current (SCLC) method. J is the current density, d is the thickness of the active layer, and $V = V_{appl} - V_r - V_{bi}$, V is the effective voltage. Hole-only devices in this work, with a structure of ITO/PEDOT:PSS/Polymer:$PC_{70}BM$/MoO_3/Al, were fabricated. Based on the equation and the $\ln(JL^3/V^2)$ vs. $(V/L)^{1/2}$ graph, the hole mobility values of PQcOx-T, PQcOx-TT, and PQcOx-biT blended with $PC_{70}BM$ were as follows: 4.18×10^{-4} cm^2V^{-1} s^{-1}, 2.39×10^{-3} cm^2V^{-1} s^{-1}, and 2.03×10^{-4} cm^2V^{-1} s^{-1}, respectively. The hole mobility of the polymers was greatly affected by the crystal structure of the polymer film, which influences the charge-transfer pathway. PQcOx-TT with face-on enriched crystallites had the highest hole mobility, which led to a high J_{SC} in the fabricated photovoltaic cell.

The active layer surface morphology is also a very critical parameter for determining the efficiency of photovoltaics. Therefore, the morphologies of the polymer/PCBM blend films were identified via AFM, as presented in Fig. 6.

The dark-colored and light-colored areas correspond to PCBM domains and polymers, respectively. The PQcOx-TT:$PC_{70}BM$ blended film has a smooth surface because of its nanoscale features and had a low root-mean-square (RMS) roughness of 0.48 nm. The

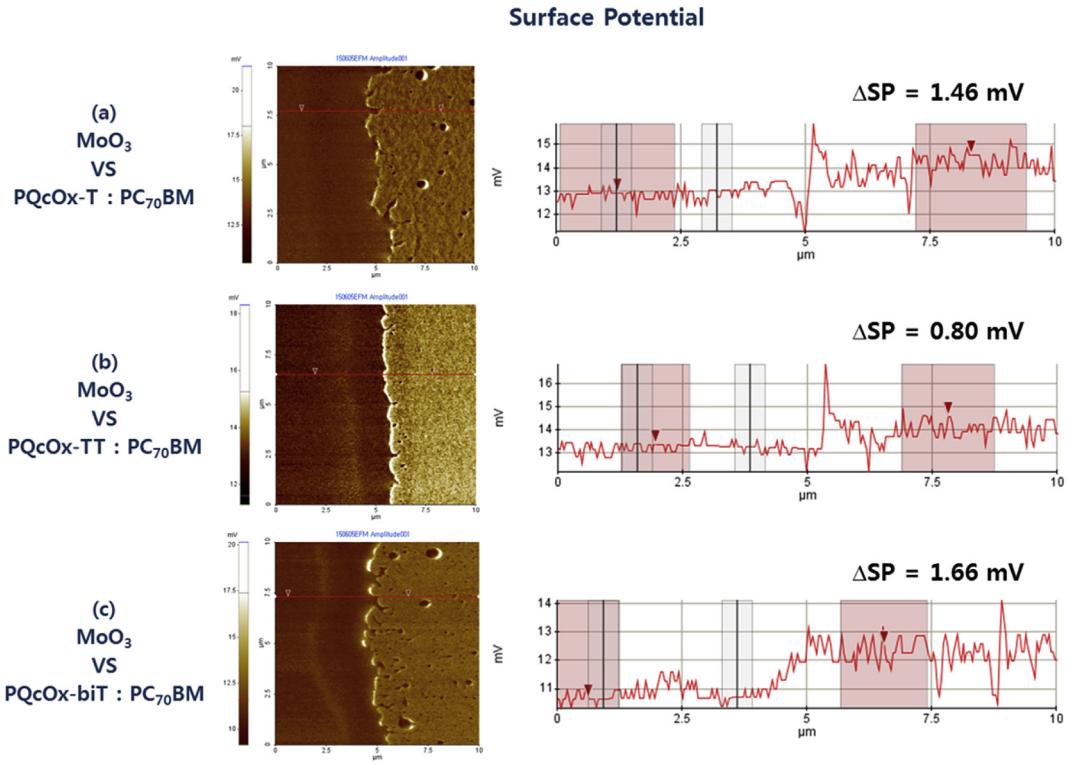

Fig. 5. Surface potential (SP) images of MoO_3 (left) and Polymer:$PC_{70}BM$ (right) and a cross-sectional line profile of the SP image (a) PQcOx-T: $PC_{70}BM$ 1:1w/w (10×10 μm^2), (b) PQcOx-TT: $PC_{70}BM$ 1:2w/w (10×10 μm^2), (c) PQcOx-biT: $PC_{70}BM$ 1:1w/w (10×10 μm^2).

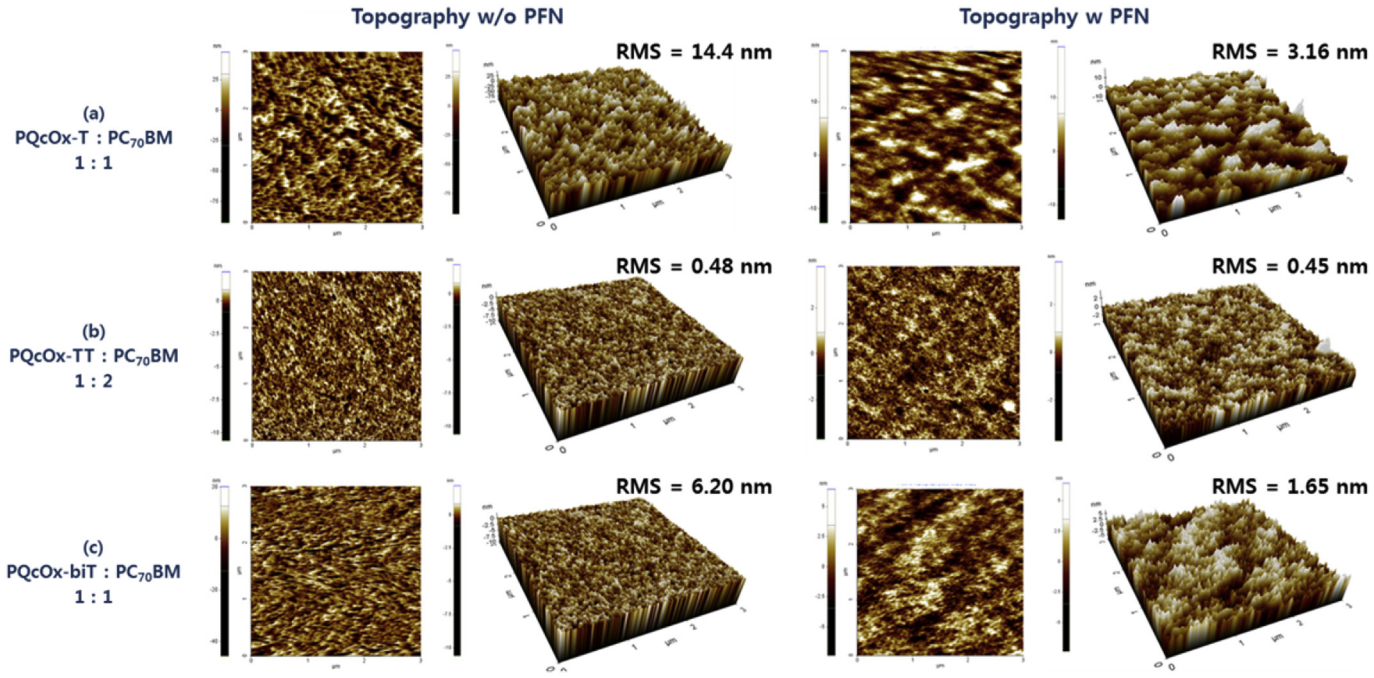

Fig. 6. Topographic AFM images of Polymer:$PC_{70}BM$ (3×3 μm^2) (a)PQcOx-T: $PC_{70}BM$ 1:1w/w, (b)PQcOx-TT: $PC_{70}BM$ 1:2w/w, (c)PQcOx-biT: $PC_{70}BM$ 1:1w/w.

good intermixing between the polymer and $PC_{70}BM$ promoted the formation of channels by the polymers. This is consistent with the high J_{sc} observed for PQcOx-TT. Black dots, which correspond to a highly aggregated PCBM domain, were observed in the PQcOx-T and PQcOx-biT:$PC_{70}BM$ blend films. In the case of PQcOx-T, in particular, large-scale phase separation was observed, and its surface was the roughest, with a root-mean-square (RMS) roughness of 14.4 nm. This is because PQcOx-T had a large steric hindrance arising from the zigzag conformation. When the PFN interlayer was introduced, the RMS of the polymer:$PC_{70}BM$ blend films decreased. This indicates that better electrode-active layer contact leads to an increase in J_{sc} and FF.

3. Experimental

3.1. Materials

2,9-diboronicester-N,N′-di(2-octyldodecyl)qui nacridone (D1) [35], 4,7-bis(5-bromothiophen-2-yl)-5,6-bis(octyloxy)benzo[c] [1,2,5]oxadiazole (A1) [37], 4,7-bis(5-bromothieno [3,2-b]thiophen-2-yl)-5,6-bis(octyloxy)benzo[c] [1,2,5]oxadiazole (A2) [22], 4,7-bis(5'-bromo-2,2'-bithiophen-5-yl)-5,6-bis(octyloxy)benzo[c] [1,2,5]oxadiazole (A3) [38] were synthesized modified procedures according to the reported procedures. The materials were purchased from the TCI, Sigma Aldrich, Alfar Aesar and Acrosor companies. Other reagents and solvents were used without further purification. Tetrahydrofuran (THF) and toluene were refluxed over benzophenone and sodium, and distilled prior to use.

3.2. General polymerizations

To a mixture of 2,9-diboronicester-N,N′-di(2-octyl-dodecyl) quinacridone (M1) (0.30 g, 0.27 mmol) and equivalent halogen compound (e.g. A1, A2 or A3), $Pd(PPh_3)_4$(0) (0.009 g, 0.008 mmol) were dissolved in 20 mL of degassed toluene under nitrogen atmosphere. 2 M degassed aqueous K_2CO_3 (10 mL) and aliquat336 compounds were placed in a Schlenk tube and was deoxygenated with nitrogen. The mixture was vigorously stirred at 90–95 °C for 48 h. After the polymerization was complete, the mixture was end-capped with 2-bromotihophene and phenylboronic acid. After the mixture was cooled to room temperature, it was poured into methanol and filtered. The filtered precipitate was further dissolved in $CHCl_3$, reprecipitated in methanol, and then filtered. The polymer was further purified by washing methanol, acetone, and chloroform, respectively, in a Soxhlet apparatus for 24 h. The chloroform part was reprecipitated with methanol, then filtrated and dried under reduced pressure at 50 °C.

3.2.1. Poly[quinacridone-alt-dithiophen-bis(octyloxy) benzo[c] 1,2,5]oxadiazole] (PQcOx-T)

Black purple solid, 0.38 g (yield = 90%). ^1H NMR (400 MHz, $CDCl_3$, d): 8.53–8.28 (m, 8H), 7.55–7.52 (m, 4H), 4.47–4.44 (m, 4H), 4.25–4.22 (m, 4H), 2.10–2.04 (m, 6H), 1.79–1.63 (m, 26H), 1.52–0.92 (m, 66H), 0.88 (s, 18H). Anal. Calcd. for $C_{70}H_{128}N_4O_5S_2$: C, 76.72; H, 9.38; N, 3.89; O, 5.55; S, 4.45. Found: C, 75.91; H, 8.84; N, 3.91; O, 5.66; S, 2.66.

3.2.2. Poly[quinacridone-alt-dithieno [3,2-b]thiophen-bis(octylxy) benzo[c] [1,2,5]oxadiazole] (PQcOx-TT)

Black purple solid, 0.25 g (yield = 78%). ^1H NMR (400 MHz, $CDCl_3$, d): 8.10–7.57 (m, 6H), 7.52–7.31 (m, 4H), 7.15–6.52 (m, 2H), 4.70–4.00 (m, 8H), 2.33–2.23 (m, 10H), 1.80–1.21 (m, 88H), 0.96–0.84 (m, 22H). Anal. Calcd. for $C_{94}H_{128}N_4O_5S_4$: Elemental Analysis: C, 74.18; H, 8.82; N, 3.60; O, 5.15; S, 8.25. Found: C, 73.54; H, 8.44; N, 3.52; O, 5.14; S, 8.43.

3.2.3. Poly[quinacridone-alt-dibithiophen-bis(octylox y)benzo[c] [1,2,5]oxadiazole] (PQcOx-biT)

Black purple solid, 0.45 g (yield = 95%). ^1H NMR (400 MHz, $CDCl_3$, d): 8.40–8.28 (m, 12H), 7.62–7.43 (m, 2H), 7.21–6.76 (m, 2H), 4.70–4.23 (m, 4H), 4.19–4.01 (m, 4H), 2.33–2.23 (m, 6H), 2.03–2.02 (m, 4H), 1.57–1.55 (m, 34H), 1.25–1.21 (m, 56H), 0.99–0.84 (m, 18H). Anal. Calcd. for $C_{98}H_{132}N_4O_5S_4$: C, 74.76; H, 8.78; N, 3.49; O, 4.98; S, 7.98. Found: C, 73.75; H, 8.18; N, 3.47; O,

5.34; S, 8.00.

3.3. Measurements

The ^{1}H NMR (400 MHz) spectra were recorded on a Brüker AMX400 spectrometer in $CDCl_3$, and the chemical shifts were recorded in units of ppm with TMS as the internal standard. The Ultraviolet–visible (UV–vis) absorption spectra of the copolymers were recorded using an Agilent 8453 UV–visible spectroscopy system. The solutions used for the UV–visible spectroscopy measurements were dissolved in chloroform at various concentrations. The films were drop-coated from the chloroform solution onto a quartz substrate. The average molecular weight and polydispersity index (PDI) of the polymers were determined using GPC analyses using THF as the eluent and a polystyrene standard as the reference. The Thermal analyses were performed using a TG 209 F3 thermogravimetric analyzer under a N_2 atmosphere. The cyclic voltammetry (CV) was produced using a Zahner IM6eX electrochemical workstation with the polymer film on a Pt plate as the working electrode, a ITO glass as the counter electrode, and silver/silver chloride [Ag in 0.1 M KCl] as the reference electrode in a 0.1 M tetrabutylammonium hexafluorophosphate (Bu_4NPF_6) acetonitrile solution. The constant scan rate was 50 mV/s. The current density–voltage (J–V) curves of the photovoltaic devices were measured by a computer controlled Keithley 2400 source measurement unit (SMU) equipped with a Class A Oriel solar simulator under an AM 1.5G illumination, 100 mW/cm^2. Atomic force microscopy (AFM) in tapping mode and electrostatic force microscopy (EFM) were performed using an XE-100 instrument under ambient conditions to obtain topographic images of the active layers and surface potentials.

3.4. Photovoltaic cell fabrication and treatment

The photovoltaic cells were constructed in the following conventional structure of ITO (170 nm)/PEDOT:PSS(40 nm)/Polymer:$PC_{70}BM$/Al(100 nm) and ITO(170 nm)/PEDOT:PSS(40 nm)/Polymer:$PC_{70}BM$/PFN(10 nm)/Al(100 nm). Poly(3,4-ethylene-dioxythiophene):poly(styrene -sulfonate) (PEDOT:PSS, from Bayer AG) was passed through a 0.45-mm filter before being spin-coated onto a cleaned ITO glass giving a thickness of about 40 nm, and then dried at 140 °C for 10 min in air. The photoactive blend layer of polymer and 1-(3-methoxycarbonyl)propyl-1-phenyl- [6,6]-C71 ($PC_{70}BM$) [1:1 (w/w), 1:2 (w/w)] was spin-coated (500–3000 rpm, 30 s) on top of the PEDOT:PSS layer (the polymer concentration of 7.5 mgmL^{-1} in chlorobenzene), and dried at 120 °C for 10 min inside a glove box. The device was completed by the deposition of a 100-nm-thick aluminum layer at pressures less than 10^{-6} torr. The active area of the device was 4 mm^2. Finally, the cell was encapsulated using UV-curing glue (Nagase, Japan). For the inverted device with the structure of ITO/ZnO (10 nm)/Polymer:$PC_{70}BM$ [1:1 (w/w), 1:2 (w/w)]/MoO_3 (5 nm)/Ag (100 nm).

3.5. Hole-only device fabrication and measurement

The hole-only devices were prepared with a diode configuration of ITO(170 nm)/PEDOT:PSS (40 nm)/Polymer:$PC_{70}BM$(50 nm)/MoO_3(30 nm)/Al(100 nm). The hole mobility of the active layers was calculated from the SCLC using the J–V curves of the hole-only devices in the dark as follows:

$$J = \frac{9}{8}\varepsilon\varepsilon_0\mu_{h(\theta)}\frac{V^2}{L^3}\exp\left(0.89\gamma\sqrt{\frac{V}{L}}\right)$$

where ε_0 is the permittivity of free space (8.85×10^{-14} F/cm); ε is the dielectric constant (assumed to be 3, which is a typical value for conjugated polymers) of the polymer; μ is the zero-field mobility of holes (electrons); L is the film thickness; and $V = V_{appl} - V_r - V_{bi}$), where V_{appl} is the applied voltage to the device, V_r is the voltage drop due to series resistance across the electrodes, and V_{bi} is the built-in voltage.

4. Conclusions

In this study, three polymers prepared with different types of spacers, poly[quinacridone-alt-spacer-bis(octyloxy)benzo[c] [1,2,5] oxadiazole] (PQcOx-T, PQcOx-TT, PQcOx-biT), were successfully synthesized by the Suzuki coupling reaction. The thiophene spacer-based polymer, PQcOx-T, adopted a zigzag conformation with a large dihedral angle between repeating units and torsion between monomer units. Furthermore, UV–vis absorption and XRD measurements showed that such a polymer exhibits an amorphous structure in the pristine polymer film. However, when thienothiophene and bithiophene spacers were introduced, the dihedral angles of PQcOx-TT and PQcOx-biT became relaxed, and a more linear conformation was observed. In particular, PQc-TT, which showed a UV–vis absorption shoulder peak in both the solution and film phases, had an oriented crystalline morphology of bimodal type XRD pattern in pristine film because of its small dihedral angle below 7°. However, in the case of PQcOx-biT, the ICT effect was unlikely to proceed smoothly and its Jsc value was decreased because the electron densities of both the ground- and excited-states existed in the same location of accepting unit. Therefore, PQcOx-TT had excellent Jsc values in the conventional cell, exhibiting a high PCE. The best performance was achieved with the PQcOx-TT:$PC_{70}BM$ structure (1:1, w/w), with a PCE value of 3.4%. In the inverted cell, PQcOx-TT had an increased Voc and FF caused by the small potential difference between the active layer and MoO_3; displayed the best performance with a PCE value of 3.6%.

Acknowledgments

This research was supported by the New & Renewable Energy Core Technology Program of the Korea Institute of Energy Technology Evaluation and Planning(KETEP) grant funded by the Ministry of Trade, industry & Energy(MI, Korea) (No. 20133030000180) and the Energy Efficiency & Resources Core Technology Program of the Korea Institute of Energy Technology Evaluation and Planning (KETEP), granted financial resource from the Ministry of Trade, Industry & Energy, Republic of Korea. (No. 20142020103970).

Appendix A. Supplementary data

Supplementary data related to this article can be found at http://dx.doi.org/10.1016/j.polymer.2016.03.062.

References

[1] F.C. Krebs, N. Espinosa, M. Hösel, R.R. Søndergaard, M. Jørgensen, Adv. Mater. 26 (1) (2014) 29–39.
[2] C.J. Brabec, S. Gowrisanker, J.J.M. Halls, D. Laird, S. Jia, S.P. Williams, Adv. Mater. 22 (34) (2010) 3839–3856.
[3] G. Yu, J. Gao, J.C. Hummelen, F. Wudl, A.J. Heeger, Science 270 (5243) (1995) 1789–1791.
[4] Y. Sun, C. Zhang, B. Dai, B. Lin, H. Yang, X. Zhang, L. Guo, Y. Liu, J. Polym. Sci. Part A Polym. Chem. 53 (16) (2015) 1915–1926.
[5] H. Zhou, L. Yang, W. You, Macromolecules 45 (2) (2012) 607–632.
[6] M. Ide, Y. Koizumi, A. Saeki, Y. Izumiya, H. Ohkita, S. Ito, S. Seki, J. Phys. Chem. C 117 (51) (2013) 26859–26870.
[7] V. Tamilavan, J. Lee, R. Agneeswari, D.Y. Lee, S. Cho, Y. Jin, S.H. Park, M.H. Hyun, Polymer 65 (2015) 243–252.
[8] U. Aygül, H. Hintz, H.-J. Egelhaaf, A. Distler, S. Abb, H. Peisert, T. Chassé, J. Phys.

Chem. C 117 (10) (2013) 4992–4998.
[9] Z. Xiao, K. Sun, J. Subbiah, T. Qin, S. Lu, B. Purushothaman, D.J. Jones, A.B. Holmes, W.W.H. Wong, Polym. Chem. 6 (12) (2015) 2312–2318.
[10] K.W. Song, M.H. Choi, H.J. Song, S.W. Heo, J.Y. Lee, D.K. Moon, Sol. Energy Mater. Sol. Cells 120 (2014). Part A:303-309.
[11] B. Yang, Y. Yuan, J. Huang, J. Phys. Chem. C 118 (10) (2014) 5196–5202.
[12] Z. He, C. Zhong, X. Huang, W.-Y. Wong, H. Wu, L. Chen, S. Su, Y. Cao, Adv. Mater. 23 (40) (2011) 4636–4643.
[13] C. Cabanetos, A. El Labban, J.A. Bartelt, J.D. Douglas, W.R. Mateker, J.M.J. Fréchet, M.D. McGehee, P.M. Beaujuge, J. Am. Chem. Soc. 135 (12) (2013) 4656–4659.
[14] M.A. Green, K. Emery, Y. Hishikawa, W. Warta, E.D. Dunlop, Prog. Photovolt. Res. Appl. 21 (1) (2013) 1–11.
[15] H.-C. Chen, Y.-H. Chen, C.-C. Liu, Y.-C. Chien, S.-W. Chou, P.-T. Chou, Chem. Mater. 24 (24) (2012) 4766–4772.
[16] H. Hu, K. Jiang, G. Yang, J. Liu, Z. Li, H. Lin, Y. Liu, J. Zhao, J. Zhang, F. Huang, Y. Qu, W. Ma, H. Yan, J. Am. Chem. Soc. 137 (44) (2015) 14149–14157.
[17] S. Ko, R. Mondal, C. Risko, J.K. Lee, S. Hong, M.D. McGehee, J.-L. Brédas, Z. Bao, Macromolecules 43 (16) (2010) 6685–6698.
[18] Y.J. Kim, Y.R. Cheon, J.-W. Jang, Y.-H. Kim, C.E. Park, J. Mater. Chem. C 3 (9) (2015) 1904–1912.
[19] N. Blouin, A. Michaud, D. Gendron, S. Wakim, E. Blair, R. Neagu-Plesu, M. Belletête, G. Durocher, Y. Tao, M. Leclerc, J. Am. Chem. Soc. 130 (2) (2008) 732–742.
[20] Z. Zeng, Y. Li, J. Deng, Q. Huang, Q. Peng, J. Mater. Chem. A 2 (3) (2014) 653–662.
[21] Q. Tao, Y. Xia, X. Xu, S. Hedström, O. Bäcke, D.I. James, P. Persson, E. Olsson, O. Inganäs, L. Hou, W. Zhu, E. Wang, Macromolecules 48 (4) (2015) 1009–1016.
[22] X. Wang, P. Jiang, Y. Chen, H. Luo, Z. Zhang, H. Wang, X. Li, G. Yu, Y. Li, Macromolecules 46 (12) (2013) 4805–4812.
[23] M.-H. Choi, K.W. Song, D.K. Moon, Polym. Chem. 6 (14) (2015) 2636–2646.
[24] V. Coropceanu, J. Cornil, D.A. da Silva Filho, Y. Olivier, R. Silbey, J.-L. Brédas, Chem. Rev. 107 (4) (2007) 926–952.
[25] M.R. Hammond, R.J. Kline, A.A. Herzing, L.J. Richter, D.S. Germack, H.-W. Ro, C.L. Soles, D.A. Fischer, T. Xu, L. Yu, M.F. Toney, D.M. DeLongchamp, ACS Nano 5 (10) (2011) 8248–8257.
[26] T. Lei, Y. Cao, X. Zhou, Y. Peng, J. Bian, J. Pei, Chem. Mater. 24 (10) (2012) 1762–1770.
[27] D. Gedefaw, M. Tessarolo, W. Zhuang, R. Kroon, E. Wang, M. Bolognesi, M. Seri, M. Muccini, M.R. Andersson, Polym. Chem. 5 (6) (2014) 2083–2093.
[28] G. Zuo, Z. Li, M. Zhang, X. Guo, Y. Wu, S. Zhang, B. Peng, W. Wei, J. Hou, Polym. Chem. 5 (6) (2014) 1976–1981.
[29] I. Osaka, M. Akita, T. Koganezawa, K. Takimiya, Chem. Mater. 24 (6) (2012) 1235–1243.
[30] MH Choi, KW Song, SW Heo, YW Han, and DK Moon. J. Ind. Eng. Chem. (0).
[31] H. Padhy, J.-H. Huang, D. Sahu, D. Patra, D. Kekuda, C.-W. Chu, H.-C. Lin, J. Polym. Sci. Part A Polym. Chem. 48 (21) (2010) 4823–4834.
[32] X. Wang, Y. Sun, S. Chen, X. Guo, M. Zhang, X. Li, Y. Li, H. Wang, Macromolecules 45 (3) (2012) 1208–1216.
[33] Z. Zhang, F. Lin, H.-C. Chen, H.-C. Wu, C.-L. Chung, C. Lu, S.-H. Liu, S.-H. Tung, W.-C. Chen, K.-T. Wong, P.-T. Chou, Energy & Environ. Sci. 8 (2) (2015) 552–557.
[34] J.-M. Jiang, P.-A. Yang, S.-C. Lan, C.-M. Yu, K.-H. Wei, Polymer 54 (1) (2013) 155–161.
[35] H. Jun Song, D. Hun Kim, M. Hee Choi, S. Won Heo, J. Young Lee, J. Yong Lee, D. Kyung Moon, Sol. Energy Mater. Sol. Cells 117 (2013) 285–292.
[36] S. Göker, G. Hızalan, Y.A. Udum, L. Toppare, Synth. Met. 191 (2014) 19–27.
[37] J.-M. Jiang, P.-A. Yang, T.-H. Hsieh, K.-H. Wei, Macromolecules 44 (23) (2011) 9155–9163.
[38] H. Yi, S. Al-Faifi, A. Iraqi, D.C. Watters, J. Kingsley, D.G. Lidzey, J. Mater. Chem. 21 (35) (2011) 13649–13656.
[39] J.-Y. Lee, M.-H. Choi, H.-J. Song, D.-K. Moon, J. Polym. Sci. Part A Polym. Chem. 48 (21) (2010) 4875–4883.
[40] C.L. Chochos, S.A. Choulis, Prog. Polym. Sci. 36 (10) (2011) 1326–1414.
[41] M.S. Almeataq, H. Yi, S. Al-Faifi, A.A.B. Alghamdi, A. Iraqi, N.W. Scarratt, T. Wang, D.G. Lidzey, Chem. Commun. 49 (22) (2013) 2252–2254.
[42] Y. Geng, J. Cong, K. Tajima, Q. Zeng, E. Zhou, Polym. Chem. 5 (23) (2014) 6797–6803.
[43] L. Biniek, B.C. Schroeder, J.E. Donaghey, N. Yaacobi-Gross, R.S. Ashraf, Y.W. Soon, C.B. Nielsen, J.R. Durrant, T.D. Anthopoulos, I. McCulloch, Macromolecules 46 (3) (2013) 727–735.
[44] W. Lee, H. Cha, Y.J. Kim, J.-E. Jeong, S. Hwang, C.E. Park, H.Y. Woo, ACS Appl. Mater. Interfaces 6 (22) (2014) 20510–20518.
[45] M. Seri, M. Bolognesi, Z. Chen, S. Lu, W. Koopman, A. Facchetti, M. Muccini, Macromolecules 46 (16) (2013) 6419–6430.
[46] J.-Y. Lee, W.-S. Shin, J.-R. Haw, D.-K. Moon, J. Mater. Chem. 19 (28) (2009) 4938–4945.
[47] H.-J. Song, D.-H. Kim, E.-J. Lee, S.-W. Heo, J.-Y. Lee, D.-K. Moon, Macromolecules 45 (19) (2012) 7815–7822.
[48] H.-J. Song, D.-H. Kim, E.-J. Lee, D.-K. Moon, J. Mater. Chem. A 1 (19) (2013) 6010–6020.
[49] H.J. Song, D.H. Kim, E.J. Lee, J.R. Haw, D.K. Moon, Sol. Energy Mater. Sol. Cells 123 (0) (2014) 112–121.
[50] M.E. Ozser, I. Yucekan, J.B. Bodapati, H. Icil, J. Lumin. 143 (0) (2013) 542–550.
[51] M. Queste, C. Cadiou, B. Pagoaga, L. Giraudet, N. Hoffmann, New J. Chem. 34 (11) (2010) 2537–2545.
[52] W. Lee, G.-H. Kim, S.-J. Ko, S. Yum, S. Hwang, S. Cho, Y.-H. Shin, J.Y. Kim, H.Y. Woo, Macromolecules 47 (5) (2014) 1604–1612.
[53] H. Zhou, L. Yang, S. Xiao, S. Liu, W. You, Macromolecules 43 (2) (2010) 811–820.
[54] M.S. Almeataq, H. Yi, S. Al-Faifi, A.A. Alghamdi, A. Iraqi, N.W. Scarratt, T. Wang, D.G. Lidzey, Chem. Commun. 49 (22) (2013) 2252–2254.
[55] X. Guo, M. Zhang, L. Huo, F. Xu, Y. Wu, J. Hou, J. Mater. Chem. 22 (39) (2012) 21024–21031.
[56] I. Osaka, M. Saito, T. Koganezawa, K. Takimiya, Adv. Mater. 26 (2) (2014) 331–338.
[57] M.-H. Choi, E.J. Ko, Y.W. Han, E.J. Lee, D.K. Moon, Polymer 74 (2015) 205–215.
[58] B.S. Ong, Y. Wu, Y. Li, P. Liu, H. Pan, Chem. Eur. J. 14 (16) (2008) 4766–4778.
[59] I. Osaka, T. Abe, S. Shinamura, E. Miyazaki, K. Takimiya, J. Am. Chem. Soc. 132 (14) (2010) 5000–5001.
[60] S. Kim, J.H. Koh, X. Yang, W.S. Chi, C. Park, J.W. Leem, B. Kim, S. Seo, Y. Kim, J.S. Yu, J.H. Kim, E. Kim, Adv. Energy Mater. 4 (6) (2014) (n/a–n/a).
[61] Y. Zhu, Z. Yuan, W. Cui, Z. Wu, Q. Sun, S. Wang, Z. Kang, B. Sun, J. Mater. Chem. A 2 (5) (2014) 1436–1442.